Robocasting of MgO doped Alumina using Alginic Acid Slurries

D. Glymond & L.J. Vandeperre

Centre of Advanced Structural Ceramics & Department of Materials, Imperial College London, South Kensington Campus, London SW7 2AZ, UK

This is the pre-peer reviewed version of the following article: Glymond D, Vandeperre LJ. Robocasting of MgO-doped alumina using alginic acid slurries. J Am Ceram Soc. 2018;00:1–8. https://doi.org/10.1111/jace.15509, which has been published in final form at http://onlinelibrary.wiley.com/doi/10.1111/jace.15509/full.

ABSTRACT

The benefits of MgO doping of alumina for maintaining a homogeneous grain structure have long been established. Therefore in this work a bespoke ink for Robocasting of alumina is developed based on the gelation of alginic acid using magnesium ions, thereby ensuring homogeneous MgO doping of the alumina green body. The shear thinning behaviour of alginic acid based solutions was paired with the rheological properties of a partially coagulated colloidal suspension to allow high solid loading inks (up to 50 vol %) with good extrusion behaviour. Shear thinning coefficients of n ~ 0.2 were recorded, with yield stresses of 250 Pa and stiffness values in the range 100-1000 kPa. The printed alumina bars reached densities of >98 % and unpolished strengths reached up to 326 ± 16 MPa after sintering at 0.4 M magnesium chloride and 45 vol% alumina.

INTRODUCTION

Additive manufacturing has been receiving large amounts of attention in recent times due to the numerous potential advantages it offers over traditional manufacturing methods for both

Author to whom correspondence should be addressed; D Glymond, email: dg2610@imperial.ac.uk

prototyping and complex shape production (1). Whilst a large amount of work has been focused on metallic and polymeric materials, more research is being focused on ceramics as applicable techniques are devised or improved upon (2, 3).

Robocasting is a direct writing technique first developed around 20 years ago (4). In contrast to other wet printing processes, such as inkjet printing that use droplet based deposition, Robocasting delivers a continuous filament through a defined shape nozzle in the desired pattern (5, 6). Filament extrusion and shape retention are controlled by tailoring the rheological behaviour of the feedstock inks, thus this can be considered to be the most important factor in the process. Aside from being homogenous and bubble free, the ink must be shear thinning to allow smooth extrusion, whilst having enough strength to both maintain its shape and support subsequent layers after being printed. Different approaches have been investigated by others in order to achieve these criteria, from inks that rely on very high solids loading so that minimal drying yields solidification (4), inks with high solvent volatility (7), inks based on the coagulation of colloidal suspensions induced by an environmental change such as pH (8) and hydrogel carriers for the ceramic particles (9). One naturally occurring gel known to have shear thinning behaviour is alginic acid and its salts (10).

Alginates are polysaccharides found in the cell walls of brown algae and are widely available as the free acid or as the sodium salt. Within the polysaccharide gel formers, alginates have the advantage that gelation is induced by an ion controlled mechanism, i.e. no temperature change is needed which keeps processing simple, unlike for example gelatin which normally needs to be kept at temperatures above 40 ^{o}C at all times to prevent gelation (11). Another advantage of the mechanism being ion controlled is the opportunity to introduce dopants to the alumina. The mechanism of alginate gelation comes from dimerization of the α-L-guluronate (G) residues in a regular two fold conformation, with interchain chelation of cations (normally calcium) to the carboxylate groups at the dimer interior, known as the “egg box” model (12). Further aggregation comes from the aggregation of the dimers themselves. The ion usually used in alginate gelation is Ca^{2+}, which gives

rapid gelation of the alginate. The use of calcium as a dopant in alumina has been shown to give exaggerated grain growth, giving poor mechanical properties (13). Robocasting using Calcium gelation of alginate has been used for high porosity biomedical applications where high temperature properties are less relevant, and where calcium is beneficial, such as bone replacement or regeneration materials (14-16). Magnesium ions (Mg^{2+}) could be a good replacement for calcium in this case as magnesium doping of alumina gives favourable microstructures (17, 18). Historically it was thought that magnesium ions do not cause alginate gelation (19). More recent findings have shown that it does in fact gel, just using a different mechanism of electrostatic interaction, and that it is much weaker and more sensitive to the structure of the alginate molecules (20). Faster gelation as well as stronger gels can be produced by increasing the alginate and Mg^{2+} concentrations (21). Hence, alginate gelled with magnesium ions appears very attractive to produce alumina parts as the MgO sintering additive for the alumina will come naturally from the gelation agent.

Mechanical properties of dense robocast ceramic material are sparse, with many researchers looking at lattices and scaffolds for biological applications rather than structural ones (22, 23). However, there are examples of robocasted high density ceramics, such as mullite (24), tricalcium phosphate (25), yttria, alumina (9) and SiC (9, 26).

In this paper the rheology, printing and sintered strength of printed magnesium doped alumina inks will be investigated, using the synergistic interaction of magnesium chloride with both the alginic acid, to form magnesium alginate, and the alumina slurry to coagulate the colloidal suspension.

EXPERIMENTAL

To prepare the inks deionised water is mixed with dispersant (Dolapix CA, Zschimmer & Schwarz, Lahnstein, Germany, 2 ml per 100 g alumina). Alginic acid (from brown algae, Sigma Aldrich, Germany) is added, and then mixed via vibratory milling to ensure homogenisation and break up of agglomerates. The alumina powder (Baikalox SMA 6, Baikowski, FR), with a d(0.5) of 0.3 μm, through

a 100 µm sieve to remove larger agglomerates and magnesium chloride (Anhydrous, Sigma Aldrich) are then added, followed by mixing and defoaming using a planetary mixer (ARE-250, Thinky, Laguna Hills, CA, USA): 3 times 2 minutes at 2000 RPM followed by 5 minutes at 2200 RPM. A range of ink formulations were tested by changing the volume fraction alumina powder added as well as the $MgCl_2$ concentration. The alginic acid concentration was set at 5 wt% relative to water, as greater concentrations made homogenisation difficult.

The rheology of the pastes was determined using a TA Instruments Discovery HR-1 rheometer with a 40 mm parallel plate geometry and a solvent trap to prevent drying. The storage and loss modulus were measured using oscillating torque and strain rate ramp experiments.

For printing, the inks are extruded using a Robocaster (3D Inks, USA) through conical nozzles with a 410 µm internal diameter at the exit. The samples were printed on a Polytetrafluoroethylene (PTFE) substrate at 65 % relative humidity to prevent drying during printing, which can cause failure of the parts due to excessive drying stress gradients. Printing extrusion was performed at 10 mm s^{-1} as it gave the best compromise between accuracy when changing direction and speed of printing. A raster pattern of filling following (9) was chosen to minimise the space between filament lines and achieve high sintered densities, with a filament spacing of 0.83 × d in the horizontal and vertical directions, with an offset of 0.5 x d between layers, where d is the nozzle diameter. The conical shaped nozzle reduces the pressure required for extrusion relative to cylindrical nozzles. The nozzle diameter was again chosen for printing speed, with each bar (5 × 4 × 30 mm) taking around 2-3 minutes to print. Printing using smaller nozzles (200 µm and 100 µm) was possible, but the pressure to extrude was towards the limit of the printer.

After drying at 30 ^{o}C in air, the sintering cycle consisted of heating at 3 ^{o}C min^{-1} to 600 ^{o}C, then heating at 5 ^{o}C min^{-1} to 1575 ^{o}C, and an isothermal holding period of 2, 5, or 10 hours before cooling at 5 ^{o}C min^{-1}. The density of the sintered bodies was determined using Archimedes' principle. The microstructure was characterised by observing thermally etched polished surfaces in a scanning

electron microscope (JEOL-5610LV, Jeol, Japan). Etching was done by exposing to 1400 ^{o}C for 30 minutes after polishing. Grain size measurements were made using Lince 2.4.2 (FG Nichtmetallische-Anorganische, TU Darmstadt, Germany). The strength of both green and sintered samples (5 × 4 × 30 mm) was measured using a 3 point bend setup on a Zwick/Roell 2.5 kN test rig. Strength tests were undertaken at 0.1 mm min^{-1}. To obtain a realistic strength value for the as-printed surfaces, the samples were not polished before testing.

RESULTS AND DISCUSSION

The rheological properties of the material can be found in Figure 1. The rheology of the inks conform well to the Herschel–Bulkley model:

$$\tau = \tau_0 + K\left(\frac{d\gamma}{dt}\right)^n$$

Each of the inks used show shear thinning behaviour (0 < n < 1) , whereby the viscosity decreases with increasing shear rates, (Figure 1A), which is important for facilitating smooth extrusion (27). Increasing the volume fraction of powder within the system increases the viscosity (and therefore extrusion pressure), but retains the thinning behaviour. The same is true for increasing the magnesium content, to a lesser extent, with a general increase of viscosity with increasing concentration of magnesium chloride additions. This is due to the Mg^{2+} ions counteracting the effect of the dispersant, which provides electrosteric stabilisation by adsorbing to the alumina particle surface. The particles then begin to agglomerate as the stability is compromised, as seen in other colloidal inks (8). Colloidal systems such as this one rely on the partial agglomeration of particles, which can lead to some inhomogeneity as seen from the deviation from linearity at higher shear rates observed in Figure 1A.

The inks also have a shear stress $\tau_0 > 0$. At stresses below the yield point they exhibit a linear response, with the storage modulus (G') and the loss modulus (G'') decreasing as the amplitude of

the stress increases towards the yield point (G' = G'') of the ink. A representative graph of the rheological data is shown in Figure 1B. The yield stresses of the inks in this study were found to be very similar, between 230 and 270 Pa, with slight increases due to alumina content and magnesium content, with the largest differences seen at 0.5 M concentration of $MgCl_2$ shown in Figure 1 C. Variation of these parameters do also change the stiffness of the inks, with increasing stiffness for both increasing magnesium content for a given alumina content, and increasing the alumina content itself, see Figure 1 D. There is a large increase in stiffness at 0.5 M $MgCl_2$ in both the 47.5 vol% and 50 vol% slurries, but not in the 45 vol% slurry, which sees a more modest stiffness increase. The reason for this has not been fully investigated, but could be due to higher powder content slurries requiring less Mg^{2+} ions to bring about destabilisation of the dispersion, as the particles are packed closer together.

High volume fractions of solids in the inks is highly desirable when printing monolithic ceramics, as it enhances the green density and therefore ability to reach full density after sintering. This along with the yield strength (τ_y) and stiffness (G') of the ink must be optimised whilst still being able to homogenise the ink easily during mixing as air bubbles can't be removed from inks, which remain too viscous during mixing. The properties shown are comparable to those of other developed ink systems for Robocasting, which have shear thinning coefficients, n, in the range 0.2 to 0.3, viscosity parameters, K, from 400 to 4000 Pa and stiffness values, G', in the range of 100-500 kPa (6-9, 26). No warpage occurs in the printed bars during drying or sintering (Figure 2). The low organic content gives the advantage of less binder burnout during the sintering step, and the high volume fraction of alumina powder ensures that drying warpage is avoided. Sintering parameters of the alumina slurries were investigated using a 45 vol% alumina 0.5 M $MgCl_2$ alginate slurry, to look at the effect of sintering hold time on the strength, since alumina fracture energy is affected by grain size, and therefore sintering time (28). Table 1 shows that the grain size, density and strength all increase with

a longer thermal hold at maximum temperature up to 10 hours. The microstructure is equiaxed as expected for magnesium doped alumina, see Figure 3.

Thus the 10 hour sintering condition was adopted for the experiments in which the effect of magnesium content and alumina loading on the mechanical properties is established. An alumina content of 45 to 50 vol% was investigated, along with a magnesium concentration of 0.1 M to 0.5 M.

The overlap of the layers is visible in a micrograph of the outer surface, Figure 4A. The fracture surface with some printing defects indicated by circles is shown in Figure 4B. Also visible at the edge of the sample is the surface roughness due to the layer-by-layer printing. Figure 4C shows that fracture is intergranular. The materials have consistently high densities across magnesium content and alumina fraction as evidenced in Table 2, with all densities recorded above 97 % and the majority above 98.5 %. The highest densities are almost theoretical, with the highest being 99.8 ± 0.1 % for the 47.5 vol% 0.1 M MgCl2 sample, before falling slightly again as the alumina and MgCl2 content increase, as increasing stiffness of the slurry causes the printing filaments to be unable to deform into the gaps between printing lines. Further optimisation of printing paths and parameters could improve this.

The highest strength (326 ± 16 MPa) was achieved with 45 vol% alumina and 0.4 M $MgCl_2$ as variables. There is a trend of decreasing strength as the alumina content is raised higher than 45 vol% with larger differences in the 0.3 M and 0.4 M samples, before beginning to converge more closely again at 0.5 M. The magnesium content trend is less simple. Aside from the reduced strength for 0.2 M Mg^{2+} in each of the volume fraction powders, for which the reason is unclear, there is an increase until 0.4 M, likely due to the increased coagulation and availability of Mg^{2+} ions for interaction with the alginate. At 0.5 M $MgCl_2$ the strength decreases again in each set of samples, which could be explained by the large increase in stiffness indicating that full coagulation has

occurred, reaching a threshold in which the filaments do not squash together as well, causing greater surface roughness and larger printing defects, as evidenced in Figure 6 and Figure 7.

For Robocasting, there are a few potential causes for critical defects with differing likelihoods; Substrate roughness, if the roughness is larger than the critical flaw size then this will limit strength, though in this case the PTFE substrate is polished to 1 µm. Thorough degassing can minimise the amount of entrapped air in the ink, but it is almost impossible to eliminate this entirely. These contribute to defects either by being incorporated into the part when extruded within the ink, or causing a sputter as they pass through the nozzle opening, leaving behind a void in the material. In extrusion based techniques, defects may be seen between the filaments if air is trapped between them during printing, if the lines do not adhere well to one another, or they are too stiff or strong to fill into all of the space. In this case the spacing of the filament lines was designed to minimise the space between lines but it was not successful in all cases, as shown in Figure 4B and Figure 6. Where the lines do touch there is good adhesion and lines are not visible as evidenced in Figure 4B, but there are sometimes defects at the triple points between filaments, with larger defects seen when the alumina volume fraction is increased, indicating that stiffness is a major contributor, if not the main one. With these defects being inside the sample, rather than on the surface, it is unlikely that they are the cause of failure for the 3 point bending tests utilised in this study, though there is likely a correlation between their size and the strength of the material, as the surface defects are very likely to be affected by the stiffness also due to the slight squashing of the filaments during extrusion to ensure high densities and to reduce cavities.

The location of the critical defect in the case of bend tests are more likely to be surface based defects. Figure 7 shows a typical fracture origin site in these materials, originating from the point between filament lines. The surface roughness is limited much to the size of the nozzle, the spacing

between filament layers and in this case the ink stiffness. Optimisation of the filament overlap could reduce some of the roughness, as well as using smaller nozzle size, but at a high cost of speed and nozzle pressure.

From the strength data the average critical defect size can be calculated using the Griffith criterion,

$$K_1 = \sigma_a \gamma \sqrt{\pi a} \text{ or } a = \frac{1}{\pi}\left(\frac{K_{iC}}{\gamma \sigma_a}\right)^2$$

Where K_1 and K_{1C} are the stress intensity and fracture toughness of the material respectively (in this case 3.5 MPa $m^{1/2}$ as described in (29)), σ is the stress, γ is a shape factor (in this case since the crack is surface based it can be approximated to be a straight plane edge crack, with a value of 1.12) and a is the critical defect size. Table 3 shows the results of this calculation for 0.4 M $MgCl_2$ samples for each of the alumina compositions. Clearly the critical defects derived from the average strength are very comparable to the size of the measured printing defects (average of 10 defects from each volume fraction), such as the ones shown in Figure 6. This further corroborates that the stiffness is directly influencing the surface roughness, and therefore the flexural strength of these materials. Nevertheless, it is worth pointing out that the strengths reported in this work compare favourably to other dense Robocasted alumina (9, 30) and are approaching the strength of higher strength alumina (up to 500 MPa) obtained via more traditional processing (29, 31).

CONCLUSIONS

A bespoke alumina ink with natural MgO doping for 3D printing using a Robocasting system was developed. The ink is based on the shear thinning behaviour of a gel of alginate added to a partially coagulated colloidal suspension. The inks exhibit shear thinning behaviour (n = 0.2), with yield

stresses of ~250 Pa and stiffnesses of 100-1000 kPa. The high solids loading (>45 vol %) reduces the shrinkage when drying, and no warping is seen after sintering. The printed alumina sinters to effectively full density, with good strengths of up to 326 ± 16 MPa without further processing or polishing after sintering. The optimum magnesium chloride concentration was found to be 0.4 M and the best volume fraction of solids 45 vol% as this provided a balance between high green densities and sufficiently low stiffness to avoid defects due to insufficient line merging.

ACKNOWLEDGEMENTS

This research was supported by Safran Power Units within the frame of the Materials and Components for Missiles, Innovation and Technology Partnership.

REFERENCES

1. Deckers J, Vleugels J, P. Kruthl J. Additive Manufacturing of Ceramics: A Review. 2014. p. 245-60.

2. Kruth JP, Leu MC, Nakagawa T. Progress in Additive Manufacturing and Rapid Prototyping. CIRP Annals - Manufacturing Technology. 1998;47(2):525-40.

3. Frazier WE. Metal Additive Manufacturing: A Review. J Mater Eng Perform. 2014;23(6):1917-28.

4. Cesarano J. A Review of Robocasting Technology. MRS Proceedings. 2011;542.

5. Cappi B, Özkol E, Ebert J, Telle R. Direct inkjet printing of Si3N4: Characterization of ink, green bodies and microstructure. J Eur Ceram Soc. 2008;28(13):2625-8.

6. Schlordt T, Schwanke S, Keppner F, Fey T, Travitzky N, Greil P. Robocasting of alumina hollow filament lattice structures. J Eur Ceram Soc. 2013;33(15–16):3243-8.

7. Lu X, Lee Y, Yang S, Hao Y, Evans JRG, Parini CG. Solvent-based paste extrusion solid freeforming. J Eur Ceram Soc. 2010;30(1):1-10.

8. Smay JE, Cesarano J, Lewis JA. Colloidal Inks for Directed Assembly of 3-D Periodic Structures. Langmuir. 2002;18(14):5429-37.

9. Feilden E, Blanca EG-T, Giuliani F, Saiz E, Vandeperre L. Robocasting of structural ceramic parts with hydrogel inks. J Eur Ceram Soc. 2016;36(10):2525-33.

10. Rezende RA, Bártolo PJ, Mendes A, Filho RM. Rheological behavior of alginate solutions for biomanufacturing. J Appl Polym Sci. 2009;113(6):3866-71.

11. Vandeperre LJ, de Wilde AM, Luyten J. Gelatin gelcasting of ceramic components. Journal of Materials Processing Technology. 2003;135(2):312-6.

12. Morris ER, Rees DA, Thom D, Boyd J. Chiroptical and stoichiometric evidence of a specific, primary dimerisation process in alginate gelation. Carbohydrate Research. 1978;66(1):145-54.

13. Dillon SJ, Harmer MP. Relating Grain-Boundary Complexion to Grain-Boundary Kinetics I: Calcia-Doped Alumina. J Am Ceram Soc. 2008;91(7):2304-13.

14. Luo Y, Zhai D, Huan Z, Zhu H, Xia L, Chang J, et al. Three-Dimensional Printing of Hollow-Struts-Packed Bioceramic Scaffolds for Bone Regeneration. ACS Applied Materials & Interfaces. 2015;7(43):24377-83.

15. Kumar A, Akkineni AR, Basu B, Gelinsky M. Three-dimensional plotted hydroxyapatite scaffolds with predefined architecture: comparison of stabilization by alginate cross-linking versus sintering. J Biomater Appl. 2015;30(8):1168-81.

16. Khalil S, Sun W. Bioprinting Endothelial Cells With Alginate for 3D Tissue Constructs. Journal of Biomechanical Engineering. 2009;131(11):111002--8.

17. Lin FJT, de Jonghe LC, Rahaman MN. Initial Coarsening and Microstructural Evolution of Fast-Fired and MgO-Doped Al2O3. J Am Ceram Soc. 1997;80(11):2891-6.

18. Bennison SJ, Harmer MP. Effect of MgO Solute on the Kinetics of Grain Growth in A12O3. J Am Ceram Soc. 1983;66(5):C-90-C-2.

19. Smidsrod O. Molecular basis for some physical properties of alginates in the gel state. Faraday Discussions of the Chemical Society. 1974;57(0):263-74.

20. Topuz F, Henke A, Richtering W, Groll J. Magnesium ions and alginate do form hydrogels: a rheological study. Soft Matter. 2012;8(18):4877-81.

21. Donati I, Asaro F, Paoletti S. Experimental Evidence of Counterion Affinity in Alginates: The Case of Nongelling Ion Mg2+. The Journal of Physical Chemistry B. 2009;113(39):12877-86.

22. Ghosh S, Parker ST, Wang X, Kaplan DL, Lewis JA. Direct-Write Assembly of Microperiodic Silk Fibroin Scaffolds for Tissue Engineering Applications. Adv Funct Mater. 2008;18(13):1883-9.

23. Franco J, Hunger P, Launey ME, Tomsia AP, Saiz E. Direct write assembly of calcium phosphate scaffolds using a water-based hydrogel. Acta Biomaterialia. 2010;6(1):218-28.

24. Stuecker JN, Cesarano Iii J, Hirschfeld DA. Control of the viscous behavior of highly concentrated mullite suspensions for robocasting. Journal of Materials Processing Technology. 2003;142(2):318-25.

25. Miranda P, Saiz E, Gryn K, Tomsia AP. Sintering and robocasting of β-tricalcium phosphate scaffolds for orthopaedic applications. Acta Biomaterialia. 2006;2(4):457-66.

26. Cai K, Román-Manso B, Smay JE, Zhou J, Osendi MI, Belmonte M, et al. Geometrically Complex Silicon Carbide Structures Fabricated by Robocasting. J Am Ceram Soc. 2012;95(8):2660-6.

27. Herschel WH, Bulkley R. Konsistenzmessungen von Gummi-Benzollösungen. Kolloid-Zeitschrift. 1926;39(4):291-300.

28. Wang J, Vandeperre LJ, Clegg WJ. Effect of Grain Size on the Fracture Behaviour of Porous Alumina Made by Partial Sintering of Powder Compacts. 25th Annual Conference on Composites, Advanced Ceramics, Materials, and Structures: B: Ceramic Engineering and Science Proceedings: John Wiley & Sons, Inc.; 2001. p. 233-41.

29. Morrell R. Handbook of properties of technical and engineering ceramics Part I. National Physical Laboratory 1985.

30. Denham HB, Cesarano III J, King BH, Calvert P, editors. Mechanical behavior of robocast alumina. Proceedings of the Solid Freeform Fabrication Symposium, Austin/TX, USA, S; 1998.

31. Auerkari P. Mechanical and physical properties of engineering alumina ceramics. Espoo, Finland: VTT; 1996.

Figures and tables

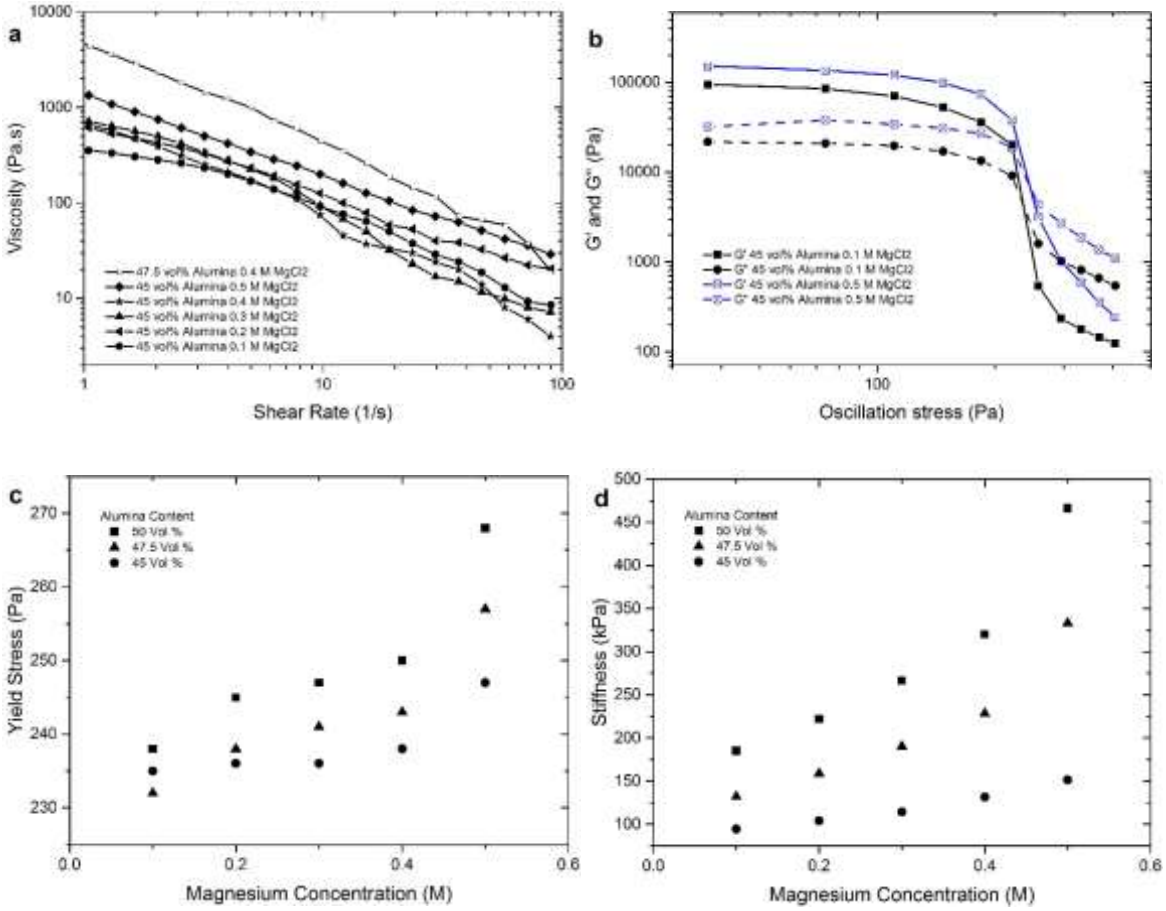

Figure 1. Rheology of the inks : a) viscosity versus shear rate, b) Storage modulus, G', and loss modulus, G'', versus oscillation stress, c) yield stress versus magnesium chloride for different alumina contents, d) stiffness versus magnesium chloride for different alumina contents.

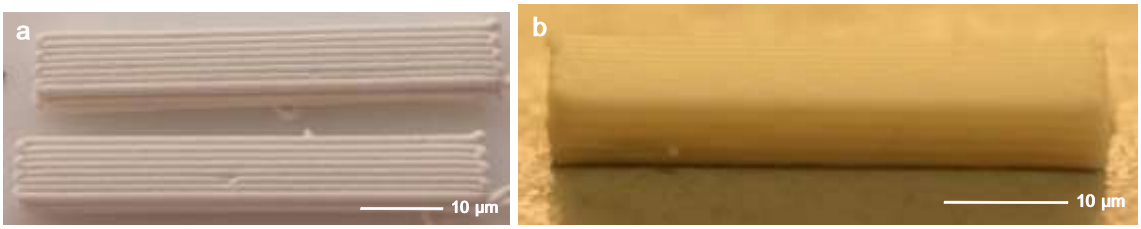

Figure 2. Photographs of a) printed (5x4x30 mm) and b) sintered bars

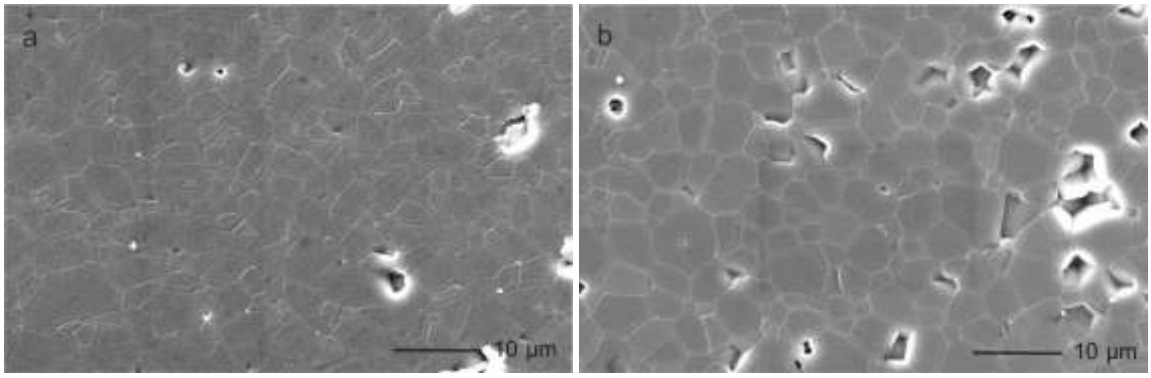

Figure 3. Micrographs of etched microstructures: a) 2 hours and b) 10 hours sintering at 1575 °C

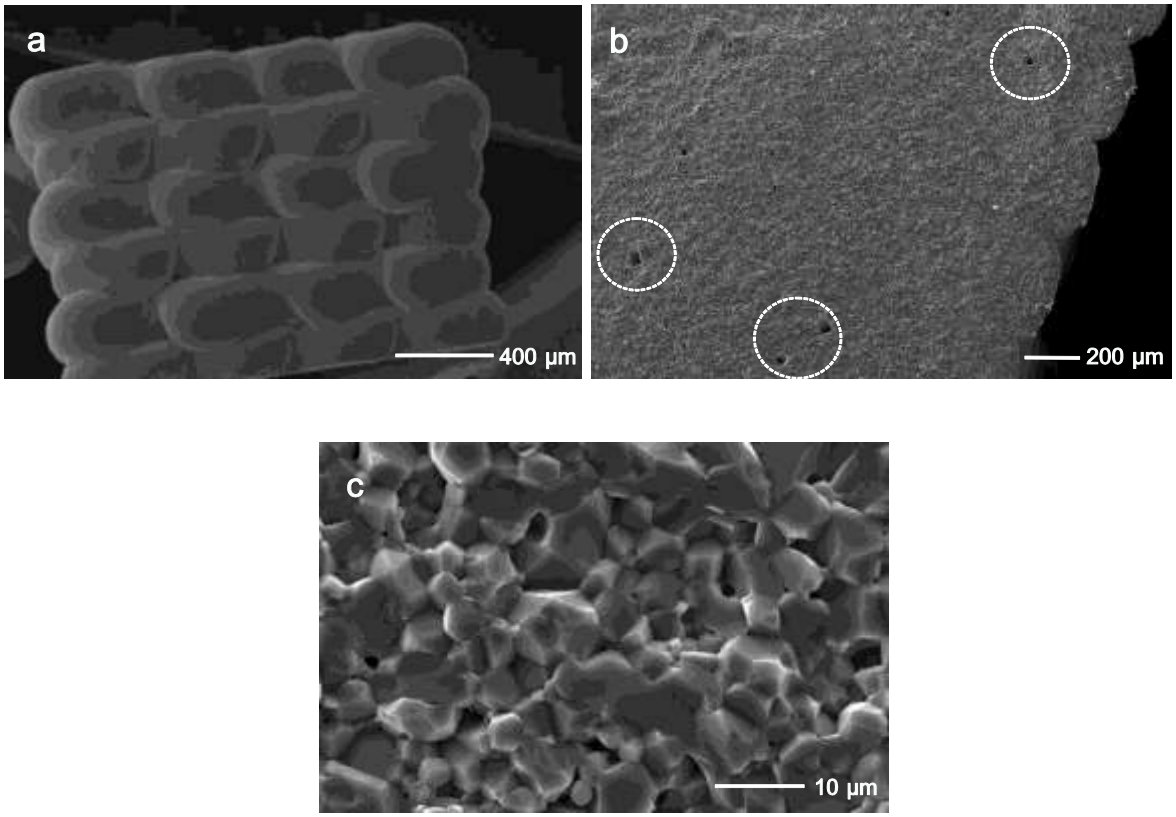

Figure 4. SEM images of a) end of bar – 47.5 vol% 0.4M. b) Fracture surface 45 vol% 0.4M, printing defects circled. Bottom c) Fracture surface 50 vol% 0.4M, showing intergranular fracture.

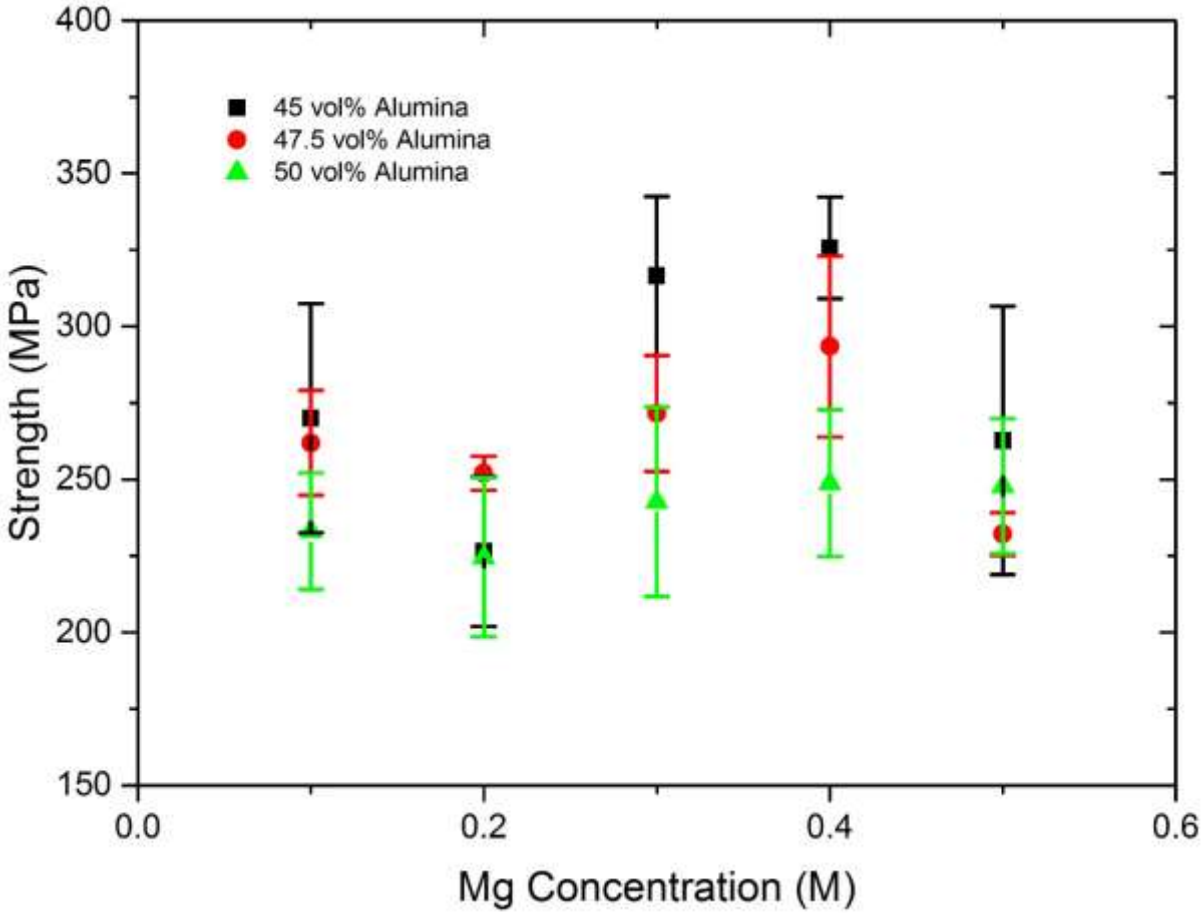

Figure 5. Strength (and standard deviation) versus magnesium concentration for solids loadings of 45, 47.5 and 50 vol%.

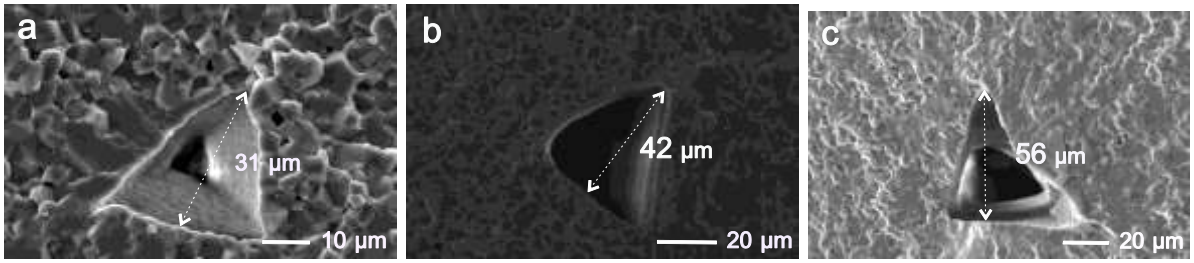

Figure 6. Example of printing defects in (all 0.4M MgCl2) a) 45 vol% alumina b) 47.5 vol% alumina and c) 50 vol% alumina

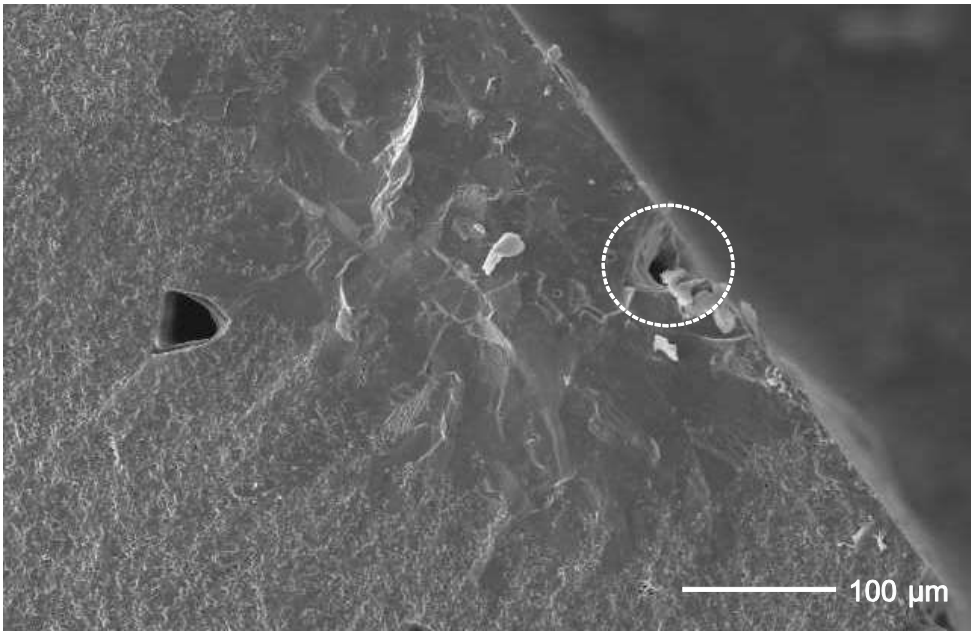

Figure 7. Typical origin of fracture in a sample, with critical defect along tensile surface of sample highlighted. Sample composition 47.5 vol% alumina 0.4 M MgCl2.

Table 1. Density and strength of samples sintered under different conditions for inks containing 45 vol% alumina, 5 wt% alginate and 0.5 M $MgCl_2$.

	Sintering Parameters		
	1575 ^{o}C 2 hours	1575 ^{o}C 5 hours	1575 ^{o}C 10 hours
Strength (MPa)	193 ± 81	228 ± 24	243 ± 20
Density	96.6 ± 0.6	97.6 ± 0.1	98.3 ± 0.1
Grain Size (μm)	3.3 ± 0.3	4.3 ± 0.2	4.6 ± 0.2

Table 2. Density versus magnesium concentration and alumina solids loading

	45 vol%	**47.5 vol%**	**50 vol%**
Mg Conc (M)		Density (%)	
0.1	98.8 ± 0.2	99.8 ± 0.1	97.7 ± 0.3
0.2	99.2 ± 0.2	99.8 ± 0.2	97.6 ± 0.4
0.3	98.5 ± 0.5	99.7 ± 0.4	98.6 ± 0.3
0.4	98.9 ± 0.4	98.8 ± 0.3	98.2 ± 0.3
0.5	98.9 ± 0.2	98.2 ± 0.3	98.4 ± 0.3

Table 3. Calculated critical defect size and measured printing defect size in 0.4M samples with varying alumina content.

Critical Defect Size (μm)	45 vol% Alumina	47.5 vol% Alumina	50 vol% alumina
Calculated	30 ± 7	39 ± 15	55 ± 5
Measured	33 ± 4	37 ± 6	59 ± 8